Hole effective mass in silicon inversion layers with different substrate orientations and channel directions.

L. Donetti and F. Gámiz

Departamento de Electrónica and CITIC, Universidad de Granada,

Avda. Fuentenueva s/n, 18071 Granada, Spain

S. Thomas, T. E. Whall, and D. R. Leadley

Nano-Silicon Group, Dept. Physics,

University of Warwick, CV4 7PE, UK

P.-E. Hellström, G. Malm, and M. Östling

ICT, Royal Institute of Technology, 16440 Kista, Sweden

Abstract

We explore the chance to define an effective mass parameter to describe hole transport in inversion layers in bulk MOSFETs and silicon-on-insulator devices. To do so, we employ an accurate and computationally efficient self-consistent simulator based on the six-band $\boldsymbol{k} \cdot \boldsymbol{p}$ model. The valence band structure is computed for different substrate orientations and silicon layer thicknesses, and is then characterized through the calculation of different effective masses taking account of the channel direction. The effective masses for quantization and density of states are extracted from the computed energy levels and subband populations, respectively. For the transport mass, a weighted averaging procedure is introduced and justified by comparing the results with hole mobility from experiments and simulations.

I. INTRODUCTION

The effective mass approximation (EMA) is a very powerful tool used to simulate and model carrier transport in semiconductor devices. The corresponding equations of motion for an electron in a periodic crystal are analogous to those of an electron in vacuum, only with a different mass. The parabolic form of the kinetic energy gives rise to simple analytic expressions for different quantities such as, for example, the density of states. Moreover, the usual Schrödinger equation is obtained when quantization is taken into account. All this allows the development of relatively fast and accurate simulation tools for silicon based electronic devices, since the approximation of the Si conduction band by parabolic valleys is reasonably good, at least for near-equilibrium properties. When non-parabolicity effects are important they can usually be treated as small corrections to the parabolic approximation obtained in a perturbative way[1,2]. Only for particular device orientations[3], or when high energy transport is studied, are more accurate approximations needed for the conduction band structure. In these cases, full-band approaches have been used[4–6].

By contrast, in the case of hole transport, the strong non-parabolicity and anisotropy of silicon valence band makes the EMA a very crude approximation. More realistic descriptions must be employed in order to obtain accurate results: some examples are the $\boldsymbol{k}\cdot\boldsymbol{p}$ model[7] or the empiric non-local pseudopotential method[8]. These approaches can accurately reproduce the valence band structure, in the full Brillouin zone or in a region of interest, using only a few parameters. The price to pay for improved accuracy is a higher computational cost and a more complex analytical form, which do not allow a simple interpretation of the results with an intuitive concept as a particle mass. Nonetheless, experimental results are often modeled or interpreted in terms of an effective mass, even in the case of holes. An intermediate approach, valid for holes in inversion layers, was developed in[9] where results obtained from a $\boldsymbol{k}\cdot\boldsymbol{p}$ model were fitted by using a semi-analytical approximation: subband levels were obtained using fitted quantization masses and the non-parabolic in-plane behavior was fitted along three different directions.

In bulk silicon, the effective mass can be computed for a given direction through the second derivative of energy around the Γ point, as set out in Table I for the three types of holes: heavy, light, and split-off. Though this mass depends on the direction and is strictly valid only in a very small region around $\boldsymbol{k} = 0$, it is usually employed for the

interpretation of experimental results[10,11]. However, as expected, other experimental data cannot be explained using such effective masses, since their validity is restricted to the neighborhood of the Γ point[12].

When carriers are confined in a two-dimensional inversion layer, as in a metal-oxide-semiconductor field effect transistor (MOSFET), different effective masses must be defined to model different properties. For electrons, this is due to the fact that the effective mass for the conduction band valleys are not isotropic; the longitudinal mass m_l and a transverse mass m_t define an effective mass tensor, whose iso-energy surfaces are ellipsoids. As a consequence, the quantization and in-plane masses of each valley depend on the relative orientation of the given valley with respect to the confinement direction. Given an arbitrary crystallographic orientation, the effective mass tensor in the device reference frame is computed, from which a quantization effective mass and the in-plane masses (transport and density of states (DOS) ones) can be obtained[13]. The quantization mass m^q is the one that appears in the Schrödinger equation and determines the energy levels and the wavefunctions of electron subbands: a large (small) mass implies low (high) energy levels and small (large) displacement of the electron distribution from the silicon–oxide interface. The DOS effective mass m_i^{DOS} is an in-plane averaged mass: it is relevant, for example, in the computation of subband population and scattering rates. The transport mass m_α depend on the channel direction (e.g. $\alpha = \langle 100 \rangle$ or $\langle 110 \rangle$): a low effective mass means large acceleration as a consequence of a drift force.

For holes in inversion layers the picture is more complex and the analogous effective masses cannot be computed because of the following issues:

i. First of all, the anisotropy of the valence band and the complex dependence of the "effective mass" on the considered direction cannot be captured by an effective mass tensor;

ii. Then, as already mentioned, the bulk "effective mass" is only valid near the Γ point, while quantization imply a non-zero value of momentum k in the confinement direction;

iii. Finally, the situation is complicated by the mixing of the three hole types produced by the interaction between the corresponding bands and the modifications induced by quantum confinement.

For all these reasons, while certainly desirable, it is not possible to follow a procedure analogous to the one used for electrons to compute the quantization, DOS, and transport

mass. We have developed an alternative procedure as follows: we simulate the properties of holes in inversion layers and extract the relevant effective masses as those parameters that allow us to model the obtained results. In particular, to compute numerically the valence band structure, we employ a self-consistent simulator based on the 6-band $\boldsymbol{k}\cdot\boldsymbol{p}$ method[7]. The self consistent simulator has been shown[14] to be accurate while at the same time computationally efficient.

The bulk effective masses of heavy, light, and split-off holes in silicon obtained with the 6 band $\boldsymbol{k}\cdot\boldsymbol{p}$ model (with parameters from Ref[15]) are reported in table I: we will discuss how the masses we obtain for holes in inversion layers compare to these bulk values. We will consider both bulk MOSFETs and Silicon-On-Insulator (SOI) devices to analyze the effect of confinement imposed by an electric field or by the geometry (the two barriers at the Si/SiO_2 interfaces), for the usual (100) surface orientation, but also for (110) and (111) orientations. In Section II we extract the quantization mass by comparing the energy levels obtained numerically for bulk MOSFETs and SOI devices with the analytical expression for triangular and square wells, respectively. In Section III, the DOS mass is computed by modeling the subband population. Then, we turn to the transport mass: we first define it in terms of the resulting energy dispersion relationships for holes in a given subband; we show that a proper averaging procedure is needed in order to define the transport mass; we support such definition with experimental results and simulations and show that carrier mobility is directly related to the proposed transport mass, and finally we summarize the main conclusions.

II. QUANTIZATION EFFECTIVE MASS

The quantization mass, m^q, is a parameter of the Schrödinger equation for electrons in a conduction band valley. In the case of the $\boldsymbol{k}\cdot\boldsymbol{p}$ model, a few material-dependent parameters are needed, but none of them can be directly related to m^q. To compute the quantization mass we first need to solve the corresponding Schrödinger-like equation numerically and then extract m^q from the results, and, to do so, we need an analytical expression with which to compare. In the case of bulk MOSFETs, the potential profile can be approximated by a triangular well[16], and the corresponding Schrödinger equation allows an analytical solution.

Energy levels E_i are given by:

$$E_i = -a_i \sqrt[3]{\frac{q^2 F^2 \hbar^2}{2m^q}}\,, \tag{1}$$

where a_i is the i-th zero of the Airy function, F is the confining electric field, and q is the absolute value of the electron charge.[17]

The resulting energy levels are plotted in Figure 1(a), (b), and (c) for (100), (110), and (111) surface orientations, respectively. Note that, in general, hole types can mix when holes are confined, so that the identification can be non-trivial in some cases. Next, the effective mass for the first subband of each of the three hole types are extracted by inverting Equation (1) with $i = 1$. The resulting masses are shown in Figure 1(d), (e), and (f), where the horizontal lines represent the bulk masses from Table I for the corresponding directions. For (100) and (111) orientations, m^q for heavy holes does not depend on the value of the electric field F and it is compatible with the bulk values. On the other hand, the mass of light holes and split-off holes varies with the electric field. The reason for such behavior can be found in the different band mixing occurring at different confinement levels. In the case of (100) orientation, the masses of light and split-off holes are similar so that a little variation is observed; however, for (111) orientation, the difference of the corresponding bulk masses is larger and the degree of mixing is higher, so that the variations of m^q with electric field are stronger; the bulk values are recovered only when the electric field tends to zero, that is in the limit of no confinement. For (110) orientation the effective mass of heavy holes also depends on the well shape, and tends to the bulk value only in the limit of weak confinement; this is a consequence of the fact that for (110) orientation, the three hole types mix strongly. Very large values (even higher than 1) of the heavy hole quantization mass are obtained even for moderate electric fields. If we repeat the procedure for the second and higher subbands of each hole band, we obtain similar but not identical results: the degree of band mixing is different and the masses do not have the same values even if the behavior is similar. However, the main conclusions are the same as before.

For fully-depleted SOI devices the simplest analytical model is the infinite square well; the energy levels for the corresponding Schrödinger equation in the EMA are given by:

$$E_i = -\frac{\hbar^2}{2m^q}\left(\frac{i\pi}{t_{\mathrm{Si}}}\right)^2, \tag{2}$$

where t_{Si} is the silicon layer thickness. If we consider the 6-band $\boldsymbol{k}\cdot\boldsymbol{p}$ model we obtain a similar result with a few differences: the split-off levels are shifted by the spin-orbit energy

and the quantization mass of each hole type is not a constant but it is a function of t_{Si}/i[18]. It means that it can depend on both the Si layer thickness and the level index i, but it is a unique function of their ratio. Next, we take into account the finite height of the potential barrier at the Si/SiO_2 interfaces by adding a small correction to the thickness. Indeed a simple quantum mechanical calculation can show that the first-order correction for finite barrier height is obtained by using a modified well width $t_{\mathrm{Si}} + \delta$, with δ proportional to $(m_h^q)^{-1/2}$. Considering all this, we can write:

$$E_{i,h} = -\frac{\hbar^2}{2m_h^q}\left(\frac{\pi}{t_i'}\right)^2 - \Delta_h, \tag{3}$$

where m_h^q is the effective mass of hole type h (heavy, light, or split-off), Δ_h is zero for heavy and light holes and equal to the spin-orbit splitting for split-off ones (44 meV for Si), and

$$t_i' = \frac{t_{\mathrm{Si}} + \delta}{i}. \tag{4}$$

Then, we compute the energy levels at flat band, when the potential profile is a square well and identify the type of each subband for different well widths. The results are shown in Figure 2(a), (b), and (c) for (100), (110) and (111) device orientations, respectively. Next, the quantization mass is extracted for each hole type as a function of t_i' by comparing the numerical results with equation (3). The results are shown in Figure 2(d), (e), and (f): we can see that as the layer thickness increases the data corresponding to different subbands and silicon thicknesses collapse to a single curve for each hole type. The outcome is quite similar to the case of the triangular well, with increasing confinement by thinner SOI layers having a qualitatively similar effect to increasing the electric field in the bulk MOSFET. The heavy hole mass is smallest for (100) devices, slightly bigger for (111) devices and much larger for the (110) ones, especially for very small t_i'. For the thickest devices (i.e. weak confinement), the effective masses reproduce the bulk values.

For both bulk MOSFETs and SOI devices the conclusions are very similar. For (100) and (111) orientations the quantization mass of heavy holes essentially coincides with the bulk mass in the $\langle 100 \rangle$ and $\langle 111 \rangle$, respectively. The mass of light holes and split-off holes can depend on the transverse electric field or the Si layer thickness; in the (100) case the variations are small because even the bulk masses values are similar to each other; in the (111) case the variations are larger, but both values are quite smaller than the heavy hole one and therefore the corresponding subbands have higher energy and, as a consequence, are

less populated. Therefore, for both (100) and (111) orientations, the bulk effective masses could provide a good approximation. On the other hand, in the case of (110) orientation, the bulk mass is recovered only for very weak confinement also for the heavy holes and quite large values of m^q are obtained for moderate confinement. In this case we expect large deviations if the bulk mass is used for models or simulations, and even a fitted value would be suitable only in a limited range of transverse electric field values and SOI layer thickness.

III. EFFECTIVE MASS FOR THE DENSITY OF STATES

For electrons in two-dimensional parabolic subbands, the density of states $g_i(E)$ is independent of energy

$$g_i(E) = \frac{m_i^{\mathrm{DOS}}}{\pi\hbar^2}, \tag{5}$$

and the occupation of a single valley reads (see for example[16]):

$$N_i = \frac{K_{\mathrm{B}}T}{\pi\hbar^2} m_i^{\mathrm{DOS}} \ln\left(1 + \exp\left(\frac{E_{\mathrm{F}} - E_i}{K_{\mathrm{B}}T}\right)\right), \tag{6}$$

where m_i^{DOS} is the DOS effective mass, K_{B} is the Boltzmann constant and E_{F} is the energy of the Fermi level in the semiconductor. For ellipsoidal valleys m_i^{DOS} can be directly computed from the in-plane masses m_x and m_y along the ellipse axes as $m_i^{\mathrm{DOS}} = \sqrt{m_x m_y}$. In the case of hole subbands we can compute the density of states numerically from the dispersion relationships $E_i(k)$ obtained by the self-consistent $\boldsymbol{k}\cdot\boldsymbol{p}$ calculation. As an example, Figure 3 shows the energy dispersion $E_1(k)$ for the fundamental subband computed for MOSFETs with the three considered surface orientations: (100), (110), and (111). The DOS obtained from the numerical $E_i(k)$ is not a constant: by directly inverting Equation (5) we would obtain an energy-dependent mass, which would not be so useful. Instead, we can compute m_i^{DOS} by inverting the hole equivalent of equation (6) to obtain:

$$m_i^{\mathrm{DOS}} = \pi\hbar^2 P_i \left[K_{\mathrm{B}}T \ln\left(1 + \exp\left(\frac{E_i - E_{\mathrm{F}}}{K_{\mathrm{B}}T}\right)\right)\right]^{-1}, \tag{7}$$

where we include the contribution of both spin states in the subband population P_i.

Figure 4(a) shows the results relative to a bulk MOSFETs as a function of inversion charge density P_{inv}, while Figure 4(b) shows m_1^{DOS} for double gate (DG) SOI devices as a function of t_{Si}. In both cases only the first subband is shown: we can observe the differences between the different substrate orientations and the variations produced by the modification of the

valence band structure under the different confining potential wells. In all cases the largest mass is obtained for (100) substrate orientation, with a value almost equal to that of the free electron mass. For (111) orientation m_1^{DOS} is smaller, and even smaller for (110) oriented devices. We have to highlight that the DOS mass implies an average in the transport plane, and it is not related to a single direction: in principle it cannot be related to the masses of Table I and, indeed, the computed values cannot be deduced from the bulk ones. When we consider the next subband the picture is even more complex: subband corresponding to the same hole type have different masses because of band mixing and the interaction (and crossings[19]) between different subbands at $k \neq 0$. For this reason and the fact that also for the fundamental subband non-trivial variations are observed, we conclude that a single value of a DOS mass cannot be provided, so that the effective mass approach cannot give accurate results for the calculation of subband population.

IV. EFFECTIVE TRANSPORT MASS

A. Orientation dependence of low-field mobility of p-channel MOSFETs

The "mass" of heavy holes is larger than that of light holes; as a consequence, confinement in MOS devices lifts their degeneracy (see Figures 1 and 2), so that the lowest energy (and most populated) subband always correspond to heavy holes. Therefore, heavy holes give the largest contribution to carrier properties, and in particular transport properties, especially at high inversion densities. Then, considering the bulk heavy hole masses for transport in the $\langle 100 \rangle$ and $\langle 110 \rangle$ directions, $m = 0.27\, m_0$ and $m = 0.54\, m_0$, respectively (see Table I), one can expect an important mobility difference between devices with $\langle 100 \rangle$ and $\langle 110 \rangle$ channel directions.

To test this experimentally, p-type MOSFETs were fabricated at KTH on 100 mm diameter silicon wafers with (100) and (110) oriented surfaces. On each wafer, MOSFETs were fabricated with channel directions along $\langle 100 \rangle$, $\langle 110 \rangle$, and a range of angles between these. Phosphorus implants formed the N-wells for the substrates, with an implant doses of 1×10^{13} cm^{-2} at 300 keV. Dry thermal oxidation for 35 minutes at 700°C was then used to grow the SiO_2 gate dielectric, on which N+ polysilicon was deposited to form the gate itself with a projected thickness of 150 nm. Source and drain regions were formed by implant-

ing with 1×10^{15} cm^{-2} of boron at 4.5 keV. A 950°C rapid thermal anneal for 30 seconds followed to activate the dopants. Connections to the gate, source, drain and substrate and their contact pads were formed by NiSi formation followed by sputtering TiW and then Al. Gate oxide thicknesses of 3.9 nm and 6.3 nm were electrically measured for the (100) and (110) p-MOSFETs, respectively, from the gate-channel capacitance in strong inversion. A substrate doping concentration of $\sim 8 \times 10^{16}$ cm^{-3} was measured from the gate-body capacitance in depletion.

In Figure 5 we show the effective mobility measured on long channel n+/SiO_2 gated p-MOSFETs for (100) and (110) substrate orientations with $\langle 100 \rangle$ and $\langle 110 \rangle$ channel directions. The effective mobility, calculated from measurements of drain current and gate-channel capacitance, is plotted as a function of inversion charge density. The inversion charge density was calculated from the gate-channel capacitance using a measurement frequency of 500 kHz. The frequency was sufficiently high that the influence of interface traps on the measurement was negligible. It was also sufficiently low to prevent distortion of the capacitance profile at low inversion charge densities caused by the high channel resistance attributed to the long channel length. In the measurement of the drain current, a drain bias of -10 mV was used. This was low enough that the error caused by the finite drain bias could be neglected in extracting the mobility. Despite these precautions, there may still be some error in the inversion charge density values calculated in the low density regime, with corresponding uncertainty in mobility values in this region.

From the results shown in Figure 5, we conclude that for (100) devices hole mobility does not depend on channel direction; it is almost the same for the $\langle 100 \rangle$ and $\langle 110 \rangle$ channels. By contrast, the hole mobility on the (110) substrate does depend on channel direction; however, the mobility along the $\langle 100 \rangle$ direction is lower than that found for the $\langle 110 \rangle$ channel orientation. This is the opposite to what one might expect given the masses of Table I, although it is consistent with results obtained by others[12]. Therefore, we can conclude that the bulk effective masses of Table I are not useful in order to understand the transport properties of differently oriented devices, and that confinement direction must also be taken into account for the computation of the transport mass.

B. Definition of the transport mass

For the transport mass, the most natural adaptation of the effective mass definition to the case of two-dimensional subbands is obtained by substituting the direction in the three-dimensional momentum space with the subband index (for quantum confinement) and the direction in the two-dimensional parallel momentum space. Thus, given the energy dispersion $E_i(k)$ of subband i, the effective transport mass m^i_α can be defined as:

$$\frac{1}{m^i_\alpha} = \frac{1}{\hbar^2}\frac{\partial^2 E_i(k)}{\partial k^2_\alpha}, \tag{8}$$

where k_α is the momentum component in the transport direction α. If the dispersion were parabolic, m^i_α would be a constant for each subband i and direction α; however, this is not the case for the subbands computed employing the $\boldsymbol{k}\cdot\boldsymbol{p}$ method, whose energy dispersion is strongly anisotropic and non-parabolic. One could take the value at $k = 0$ as a representative value[18,20]. However $m^i_\alpha(k)$ can present strong variations as a function of k and, moreover, the functional dependence on k can depend on the confining potential (silicon layer thickness in SOI devices and applied bias). As an example, Figure 6 shows $m^1_{\langle 110\rangle}$ along the $\langle 110\rangle$ direction for (110) oriented SOI devices with different silicon thicknesses. There are strong variations in the effective mass, which get larger for the thicker devices: the behavior strongly depends on t_{Si}, while the value at $k = 0$ only presents a weak dependence. This means that the different behavior one expects due to the differences in the energy dispersion is not captured by the value of $m^1_{\langle 110\rangle}$ at $k = 0$.

When we consider the wave-vector k in the whole two-dimensional transport plane the picture is even more complex, as shown in Figure 7. Figures 7(a) and (b) show the inverse effective mass computed as in Equation (8) for a SOI device ($t_{\mathrm{Si}} = 2$ nm) with (100) orientation and $\langle 100\rangle$ and $\langle 110\rangle$ transport direction, respectively. The values near the Γ point are similar in the two cases, while in the rest of the k-plane the behavior is completely different and the variations of effective mass even in a relatively small region are important. Figures 7(c) and (d) show the same quantity for a (110) substrate and the same $\langle 100\rangle$ and $\langle 110\rangle$ directions: again, the variations are very strong and the behavior is completely different. Finally, Figures 7(e) and (f) correspond to devices with the same (110) orientation and $\langle 110\rangle$ channel as in (d) but with $t_{\mathrm{Si}} = 3$ nm and $t_{\mathrm{Si}} = 5$ nm, respectively. The value near the Γ point is similar in the three cases, while the behavior in the rest of the k-plane is different, as was the case for the one-dimensional dependence shown in Figure 6. Therefore, to take into

account the contribution of all the occupied region of momentum space at equilibrium, we define an average effective transport mass M_α^i, where the weight is given by the occupation probability. We obtain[21]:

$$\frac{1}{M_\alpha^i} = \left\langle \frac{1}{m_\alpha^i} \right\rangle = \int \frac{f\left(E_i(k)\right)}{m_\alpha^i} dk \Bigg/ \int f\left(E_i(k)\right) dk, \tag{9}$$

where $f(E)$ is the Fermi-Dirac distribution function.

An important observation is that M_α^i does not depend on the direction α in the transport plane when substrate orientation is (100) or (111). For example, for (100) devices, $M_{[010]}^i$ and $M_{[001]}^i$ coincide for symmetry reasons. Then we have

$$\begin{aligned}
\frac{1}{M_\alpha^i} =& \frac{1}{\hbar^2} \left\langle \frac{\partial^2 E_i(\boldsymbol{k})}{\partial k_\alpha^2} \right\rangle_i \\
=& \frac{1}{\hbar^2} \left\langle \frac{\partial^2 E_i(\boldsymbol{k})}{\partial k_{[010]}^2} \right\rangle_i \cos^2\alpha + \frac{1}{\hbar^2} \left\langle \frac{\partial^2 E_i(\boldsymbol{k})}{\partial k_{[001]}^2} \right\rangle_i \sin^2\alpha + \frac{1}{\hbar^2} \left\langle \frac{\partial^2 E_i(\boldsymbol{k})}{\partial k_{[010]} \partial k_{[001]}} \right\rangle_i \cos\alpha \sin\alpha \\
=& \frac{1}{M_{[010]}^i} \cos^2\alpha + \frac{1}{M_{[001]}^i} \sin^2\alpha \\
=& \frac{1}{M_{\langle 100 \rangle}^i},
\end{aligned} \tag{10}$$

where the average of the mixed derivative vanishes for symmetry reasons and the last line follows from the fact that $M_{[010]}^i = M_{[001]}^i = M_{\langle 100 \rangle}^i$. An analogous proof is possible in the case of (111) surface orientation. This fact can explain the very small dependence on channel orientation observed for the mobility on (100) substrates shown previously. Taking into account the observed difference between $m_{\langle 100 \rangle}^i$ and $m_{\langle 110 \rangle}^i$ as functions of k, as shown in Figures 7(a) and (b), we can conclude that averaging is crucial in order to obtain the in-plane isotropic behavior of M_α^i.

We stress that the proposed averaging procedure is different from the one proposed in Ref.[12] to explain similar experimental results. In that case, the authors calculated the effective mass (Equation (8)) at $k = 0$ for all directions α and then averaged over α, justifying such average by the fact that in near equilibrium (long channel devices) all two-dimensional momentum space must contribute to the "sampled" effective mass. On the contrary, we calculate the directional derivative as a function of k for a given α and average these values in the whole two-dimensional k plane (weighted by hole population). The reason is that

the wave-vector k can take every direction in the transport plane, but α is fixed because it represents the channel direction, *i.e.* the direction of the drift electric field: the (second) derivative along a given direction α represents the effect that an electric field in such direction has on the motion of a carrier with given wave-vector k.

In Figure 8, we show $M^1_{\langle 100\rangle}$ and $M^1_{\langle 110\rangle}$ computed according to equation (9), for p-channel MOSFETs with (100) and (110) substrate orientations, as a function of inversion carrier density. Comparing these results with the measured effective mobility of Figure 5, we can see that the average effective mass is useful in order to interpret the experimental results. Firstly, we note that in the high inversion charge density region, where practical devices operate, the mass is significantly lower for (110) orientated substrates than for (100) orientation. This can directly explain the enhanced mobility observed on (110), which has previously been attributed to reduced scattering arising from a greater subband splitting between light and heavy holes. Secondly, for (100) substrate orientation, the transport mass does not depend on channel direction, as expected from symmetry arguments. Thirdly, for (110) orientation, the transport mass is lower for both channel directions: in particular, $M^1_{\langle 110\rangle}$ is lower than $M^1_{\langle 100\rangle}$ (except at very low inversion charge density) and this fact agrees with the higher mobility observed for the $\langle 110\rangle$ channel. Moreover, the masses for the two directions get closer to each other at small values of inversion charge, where the mobility values also converge. This analysis is not fully comprehensive, because it only takes into account the first subband of heavy holes, but shows that the average transport mass defined in equation (9) is useful for the interpretation of transport properties near equilibrium.

C. Simulation study of hole mobility of ultra-thin SOI devices

Now, we turn to ultra-thin SOI devices and consider the dependence of hole mobility on orientation and Si film thickness, and its relation to the transport effective mass. To do so, we simulate different symmetric DG SOI structures with silicon layer thicknesses, $t_{\rm Si}$, ranging from 1 to 15 nm; the channel is considered essentially undoped ($N_D = 1 \times 10^{14}$ cm^{-3}), the thickness of both oxide layers is $t_{\rm ox} = 1$ nm, and a midgap metal is used as a gate material. We compute the hole mobility, μ, employing the Kubo-Greenwood formula[22], employing the subband dispersion and wavefunctions obtained with the 6 band $\boldsymbol{k}\cdot\boldsymbol{p}$ model, as in Ref.[14]. We take into account phonon (optical and acoustic) and surface roughness (SR) as scattering

mechanisms[23].

The dependence of hole mobility on t_{Si} is shown in Figure 9, for different values of inversion carrier density P_{inv}. We only represent one curve for (100) and (111) surface orientations, because in these cases μ shows a very small dependence (up to 1–2%) on channel orientation, whereas a large mobility difference is observed between different channel orientations for (110) devices. It is clear that for very thin channels μ is always strongly reduced; however, it is important to emphasize that there are large quantitative differences between curves corresponding to different surface and channel orientations. The most important observation is that hole mobility is severely degraded for (100) devices below 6 nm, while this happens at smaller values of t_{Si} for (110) and (111) devices. Therefore, the mobility enhancement of alternative orientations not only persists for ultra-thin devices; on the contrary, it increases and can be quite large, especially at small values of P_{inv}. To study the origin of such enhancement we separate the mobility of the first two subbands, as shown in Figure 10. The important mobility decrease can be attributed to the increase of both phonon and surface roughness (SR) scattering at small Si thickness. One difference that Figure 10 highlights at small t_{Si} is an enhanced mobility in the second subband for (111) orientation compared to (100), which may go someway to explaining the shape of Figure 9. This is less pronounced for (110). However, the different behavior corresponding to different surface orientations cannot be fully explained by differences in the scattering rates[21].

Figure 11 shows m_α^1 computed at $k = 0$ and M_α^1 as functions of t_{Si}; while the former has a weak dependence on t_{Si} for all orientations, the latter shows a strong decrease at small t_{Si} for (110) surface orientation, especially for the $\langle 110 \rangle$ direction. This fact compensates, to a certain extent, the large increase of scattering rates (both from phonons and SR) occurring at very small thicknesses, giving rise to the mobility behavior shown in Figures 9 and 10. Such a decrease of M_α^1 is not caused by a corresponding decrease in $m_\alpha^1(0)$ but, as we can see in Figures 7(d), (e), and (f) by a flattening of the surface of $m_\alpha^1(k)$. Figure 11 also shows that M_α^i for (110) substrate orientation is lower than (100) or (111) orientations and that, in this case, it depends on the transport direction: in particular the effective mass for the $\langle 110 \rangle$ channel is much lower (and consequently the mobility is larger) than for the $\langle 100 \rangle$ channel.

To conclude this section, we can say that the mobility advantage of (110) over (100) substrates, observed for bulk MOSFETs and thick SOI ones, gets larger for very thin SOI

structures. The behavior of the transport mass, defined with the proper averaging procedure, is very useful in interpretting this result.

V. CONCLUSIONS

We have explored the chance to define an effective mass for hole transport for both bulk and ultra-thin SOI inversion layers, and we have also provided a procedure to evaluate such a parameter, when it is possible. We have shown how to compute the quantization mass, DOS mass and transport mass for holes in bulk and SOI MOSFETs; in particular, the transport mass can be related to transport properties only if proper averaging is taken into account. The "bulk" hole mass can be used as the quantization mass only for heavy holes in devices with (100) and (111) orientations. In the cases of DOS and transport mass there is no direct relationship with the "bulk" ones, and those must be computed from the numerical band structure. The results can be used to explain why hole transport is most favorable for a $\langle 110 \rangle$ directed channel on a (110) orientated substrate.

ACKNOWLEDGMENTS

This work was partially supported by the EU EUROSOI+ Thematic Network (FP7-CA-216373) and "NANOSIL" Network of Excellence (FP7 IST-216171). The work of L.D. is done as part of the program Ramón y Cajal of the Ministerio de Ciencia e Innovación (M.C.I.) of Spain. Financial support from M.C.I. (contracts TEC2008-06758-C02-01 and FIS2008-05805), Junta de Andalucía (project TIC-P06-1899).

---

[1] M. V. Fischetti and S. E. Laux, Physical Review B **48**, 2244 (1993).

[2] C. Jungemann, A. Emunds, and W. Engl, Solid-State Electronics **36**, 1529 (1993).

[3] K. Uchida, A. Kinoshita, and M. Saitoh, in *Electron Devices Meeting, 2006. IEDM '06. International* (2006) pp. 1–3.

[4] K. Hess, *Monte Carlo device simulation: full band and beyond* (Kluwer, 1991).

[5] A. Abramo, L. Baudry, R. Brunetti, R. Castagne, M. Charef, F. Dessenne, P. Dollfus, R. Dutton, W. Engl, R. Fauquembergue, C. Fiegna, M. Fischetti, S. Galdin, N. Goldsman, M. Hackel,

C. Hamaguchi, K. Hess, K. Hennacy, P. Hesto, J. Higman, T. Iizuka, C. Jungemann, Y. Kamakura, H. Kosina, T. Kunikiyo, S. Laux, H. Lin, C. Maziar, H. Mizuno, H. Peifer, S. Ramaswamy, N. Sano, P. Scrobohaci, S. Selberharr, M. Takenaka, T. Tang, K. Taniguchi, J. Thobel, R. Thoma, K. Tomizawa, M. Tomizawa, T. Vogelsang, S. Wang, X. Wang, C. Yao, P. Yoder, and A. Yoshii, IEEE Transactions on Electron Devices **41**, 1646 (1994).

[6] M. V. Fischetti and S. E. Laux, Physical Review B **38**, 9721 (1988).

[7] J. M. Luttinger and W. Kohn, Physical Review **97**, 869 (1955); J. M. Luttinger, *ibid.* **102**, 1030 (1956).

[8] J. R. Chelikowsky and M. L. Cohen, Physical Review B **14**, 556 (1976).

[9] M. De Michielis, D. Esseni, Y. Tsang, P. Palestri, L. Selmi, A. O'Neill, and S. Chattopadhyay, Electron Devices, IEEE Transactions on **54**, 2164 (2007).

[10] T. Mizuno, N. Sugiyama, T. Tezuka, Y. Moriyama, S. Nakaharai, T. Maeda, and S. Takagi, in *IEEE International Electron Devices Meeting, Tech. Dig. 2003* (2003) pp. 33.6.1– 33.6.4.

[11] S. Takagi, M. Takayanagi, and A. Toriumi, Electron Devices, IEEE Transactions on **46**, 1446 (1999).

[12] S. Saito, D. Hisamoto, Y. Kimura, N. Sugii, R. Tsuchiya, K. Torii, and S. Kimura, in *VLSI Technology, 2006. Digest of Technical Papers. 2006 Symposium on* (2006) pp. 150–151.

[13] A. Rahman, M. S. Lundstrom, and A. W. Ghosh, Journal of Applied Physics **97**, 053702 (2005).

[14] L. Donetti, F. Gamiz, and N. Rodriguez, Semiconductor Science and Technology **24**, 035016 (2009).

[15] M. V. Fischetti and S. E. Laux, Journal of Applied Physics **80**, 2234 (1996).

[16] F. Stern and W. E. Howard, Physical Review **163**, 816 (1967).

[17] Only in this case we do not impose self-consistency in our simulations; energy levels are computed for triangular well with varying electric field and for different quantization directions.

[18] Y. Kajikawa, Journal of Applied Physics **106**, 063712 (2009).

[19] Y. Zhang, J. Kim, and M. Fischetti, Journal of Computational Electronics **7**, 176 (2008).

[20] E. Wang, P. Matagne, L. Shifren, B. Obradovic, R. Kotlyar, S. Cea, M. Stettler, and M. Giles, Electron Devices, IEEE Transactions on **53**, 1840 (2006).

[21] L. Donetti, F. Gámiz, N. Rodríguez, F. Jiménez-Molinos, and J. Roldán, Solid-State Electronics **54**, 191 (2010).

TABLE I. Effective masses computed for bulk Si with the 6-band $\boldsymbol{k}\cdot\boldsymbol{p}$ model for different channel directions.

	$\langle 100\rangle$	$\langle 110\rangle$	$\langle 111\rangle$
heavy holes	0.274	0.541	0.668
light holes	0.204	0.149	0.142
split off holes	0.234	0.234	0.234

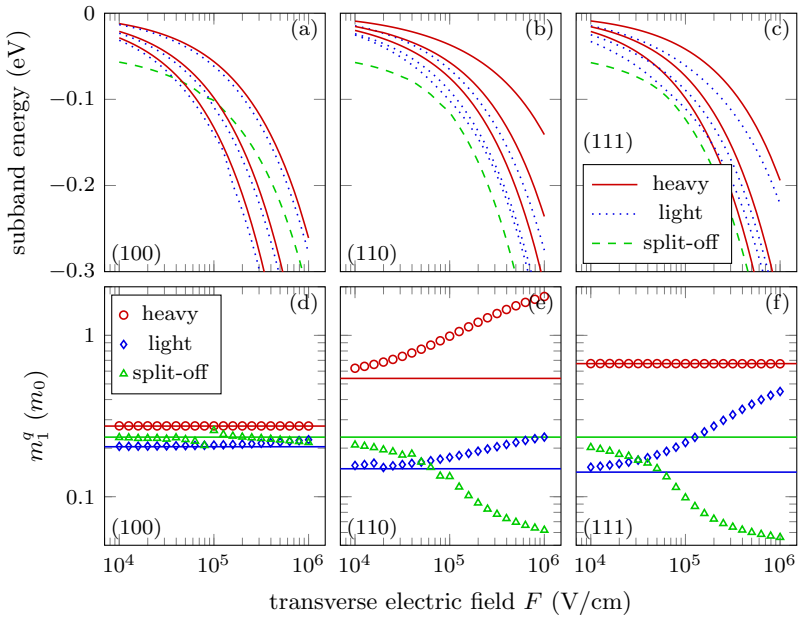

FIG. 1. (Color online) Energy level and quantization mass for holes in a triangular well, as a function of the transverse electric field for surface orientations (100), (110) and (111).

[22] M. V. Fischetti, Z. Ren, P. M. Solomon, M. Yang, and K. Rim, Journal of Applied Physics **94**, 1079 (2003).

[23] L. Donetti, F. Gamiz, N. Rodriguez, A. Godoy, and C. Sampedro, Journal of Applied Physics **106**, 023705 (2009).

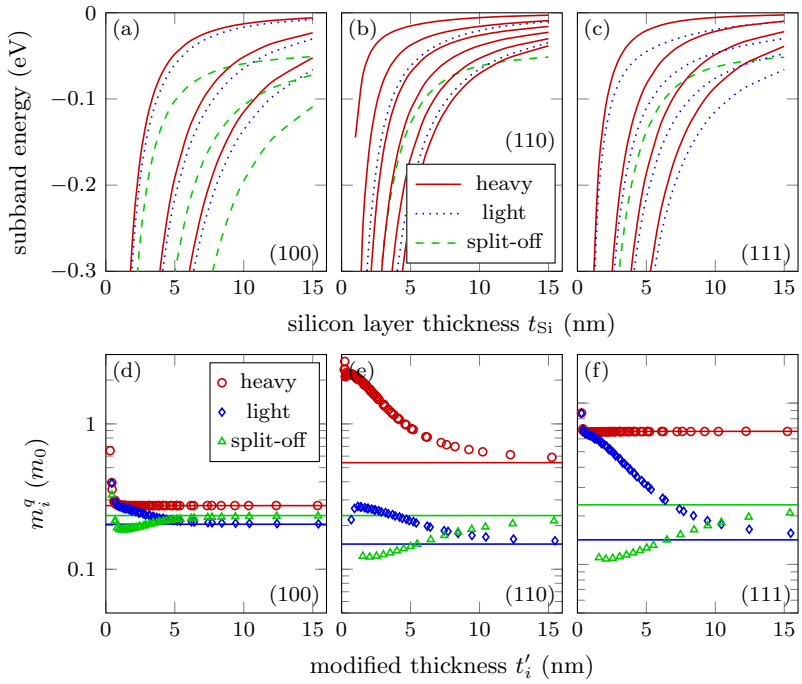

FIG. 2. (Color online) Energy level and quantization mass for SOI devices, as a function of the silicon layer thickness for different surface orientations.

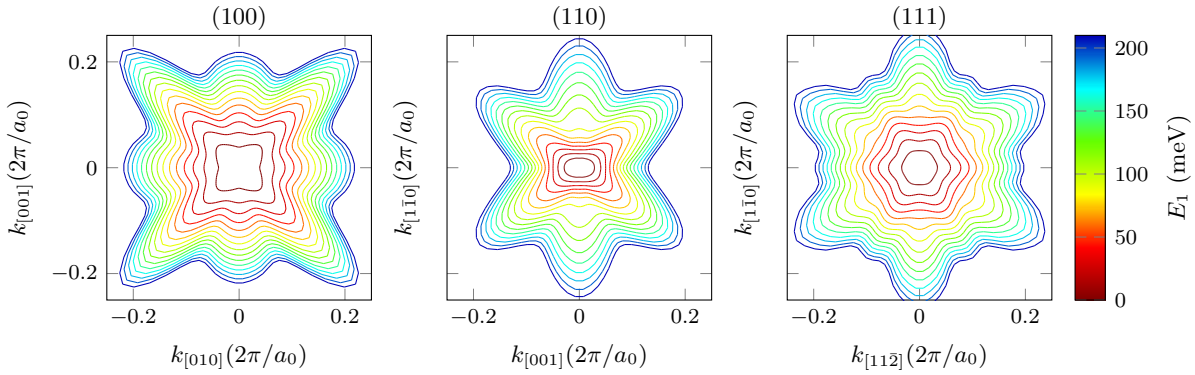

FIG. 3. (Color online) Energy dispersion $E_1(k)$ for the fundamental subband in (100), (110), and (111) MOSFETs with inversion density $P_{\mathrm{inv}} = 6 \times 10^{12}$ cm^{-2}. The energy difference between contour levels is 15 meV.

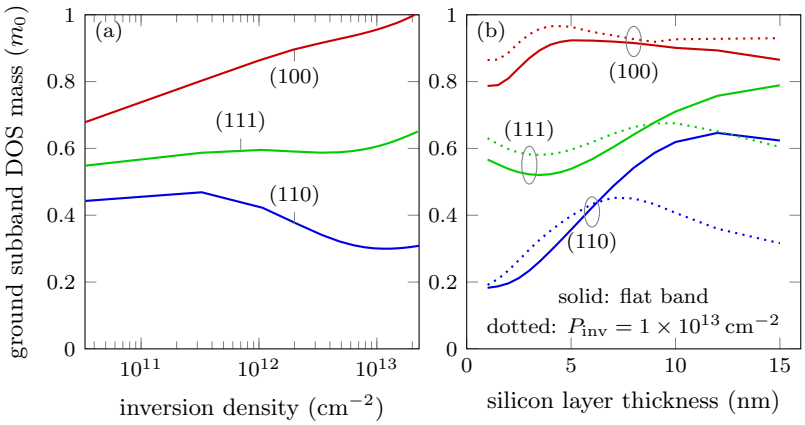

FIG. 4. (Color online) DOS effective mass of the fundamental subband of bulk MOSFETs (a) and DG SOI devices (b).

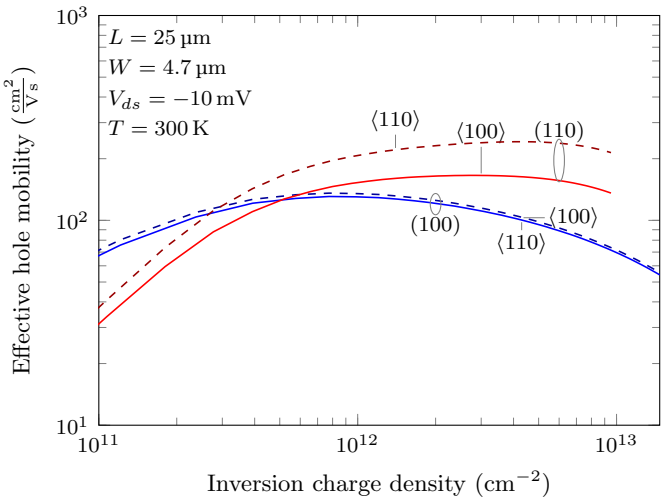

FIG. 5. (Color online) Hole effective mobility as a function of inversion charge density, for (100) and (110) substrates and channel orientations along ⟨100⟩ and ⟨110⟩.

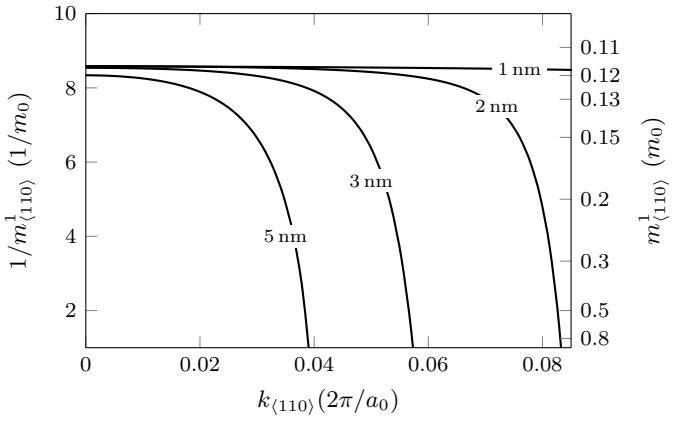

FIG. 6. Transport mass $m^1_{\langle 110\rangle}$ of the first subband along $\langle 110\rangle$ direction for (110) oriented SOI devices with different silicon thicknesses.

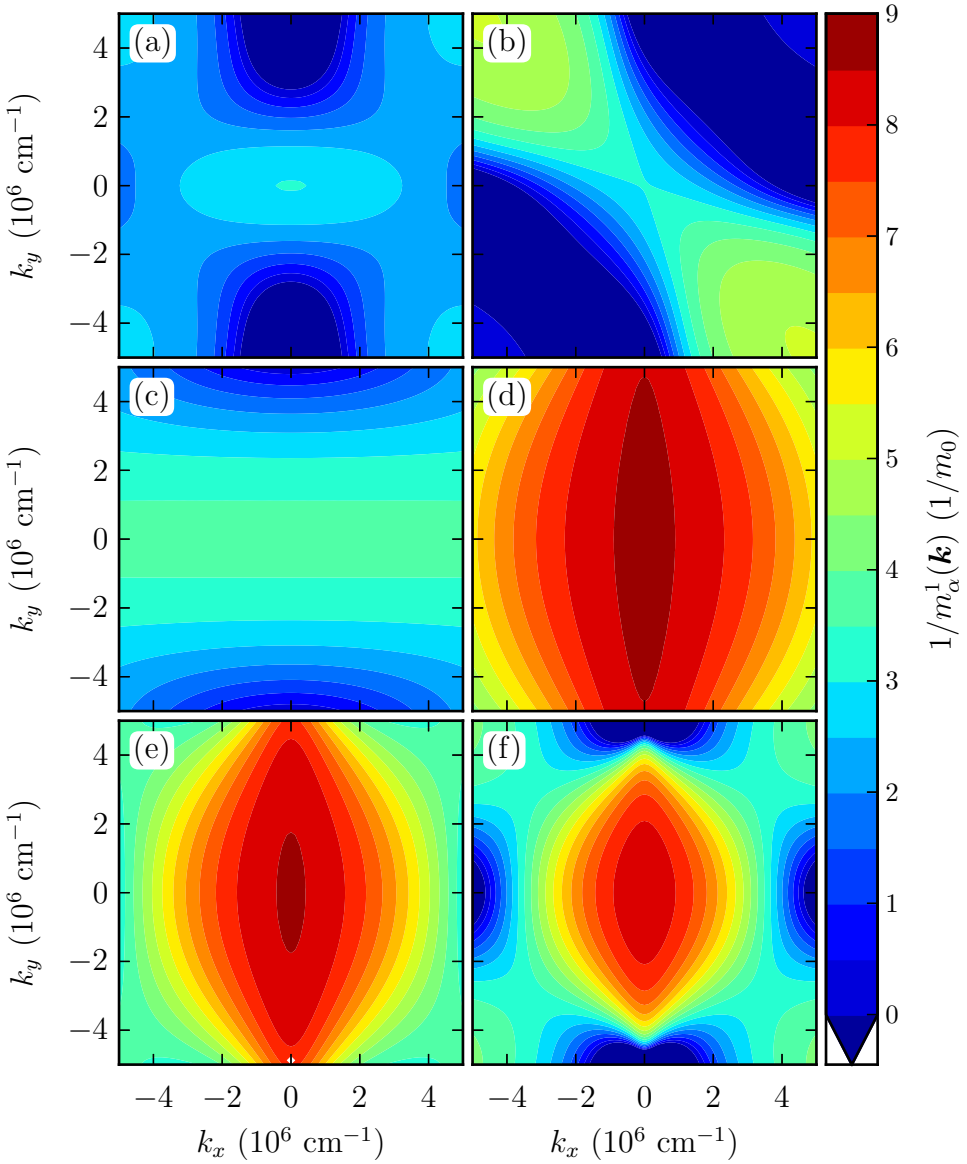

FIG. 7. (Color online) Transport mass m^1_α as a function of k for the following SOI devices: $t_{\mathrm{Si}} = 2$ nm with (100) surface orientation and k_α parallel to $\langle 100\rangle$ (a), (100)/$\langle 110\rangle$ (b), (110)/$\langle 100\rangle$ (c), (110)/$\langle 110\rangle$ (d); (e) and (f) are the same as (d) but with $t_{\mathrm{Si}} = 3$ nm and 5 nm, respectively. For (100) orientation k_x and k_y are directed along [010] and [001], while for (110) orientation they are directed along [001] and $[1\bar{1}0]$.

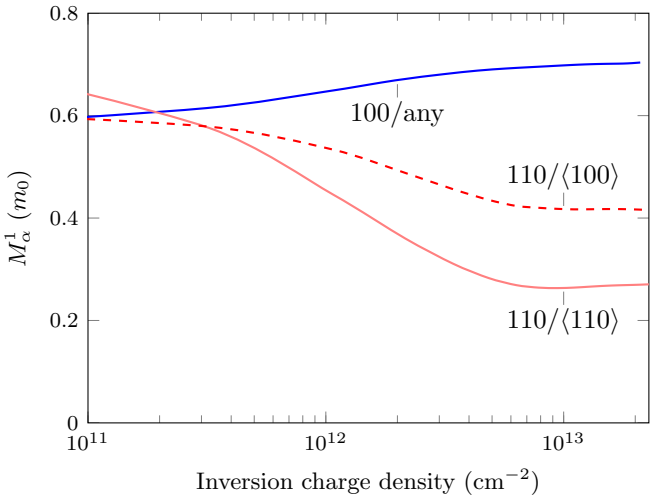

FIG. 8. (Color online) Average hole transport mass M_α^1 of the first subband along $\langle 100 \rangle$ and $\langle 110 \rangle$ directions for (100) and (110) oriented p-MOSFETs.

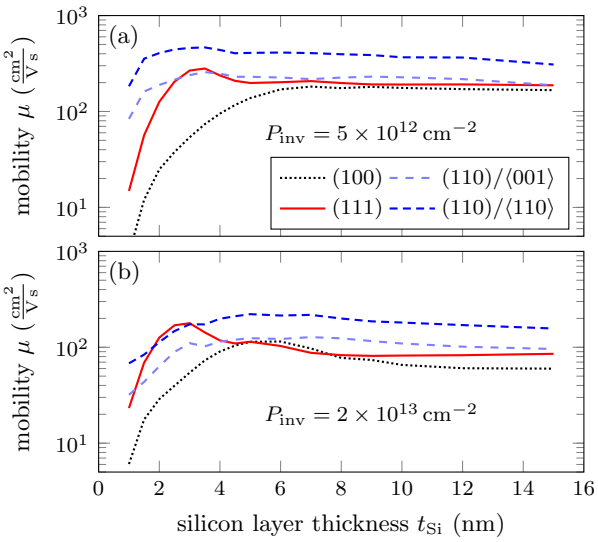

FIG. 9. (Color online) Calculated hole mobility as a function of t_{Si} for different surface orientations and channel directions.

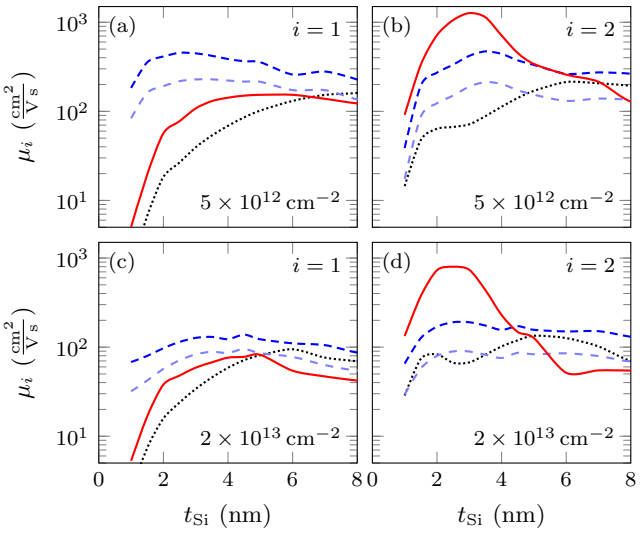

FIG. 10. (Color online) Calculated mobility of holes in the first and second subbands. Line types and colors represent surface orientations and channel directions as in Figure 9.

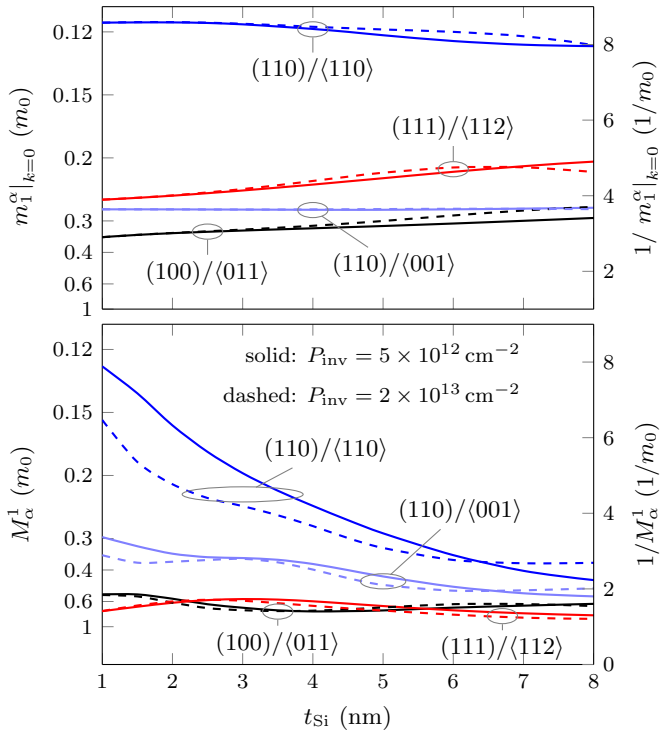

FIG. 11. (Color online) Effective masses $m_\alpha^1(0)$ and M_α^1 as a function of t_{Si} for SOI devices with different substrate orientations and channel directions.